

Influence of hydroxyapatite on maghemite-to-hematite phase transfer of FeO_x-hydroxyapatite composite

Kunfeng Zhao · Xin Liu · Changzi Jin · Fuhai Yu ·
Alexandre Rykov · Junhu Wang · Tao Zhang

© Springer Science+Business Media Dordrecht 2012

Abstract FeO_x-hydroxyapatite (FeO_x-HAP) composites with different FeO_x contents were prepared, and compared with pure FeO_x, the FeO_x-HAP composites exhibit strongly magnetic behavior in an external magnetic field even after 600 °C calcination. The combination of ⁵⁷Fe Mössbauer and Fe K-edge XAFS indicates that HAP can stabilize the size and crystal phase of γ-Fe₂O₃ during heat treatment. Even after 600 °C calcination, the interaction imposed by HAP could produce large amounts of distorted octahedral coordination Fe sites in the interior lattice and then result in strong magnetism. The thermally stable γ-Fe₂O₃-HAP composites may provide a new opportunity for developing efficient supported crystal-dependent catalysts.

Keywords FeO_x-hydroxyapatite · Crystal phase transfer · Thermal stability · Mössbauer · XAFS

1 Introduction

In recent years, magnetic iron oxide nanoparticles have been extensively employed as catalyst supports especially in liquid phase catalysis in consideration of their facile

K. Zhao · X. Liu · C. Jin · F. Yu · J. Wang (✉) · T. Zhang (✉)
State Key Laboratory of Catalysis, Dalian Institute of Chemical Physics,
Chinese Academy of Sciences, 457 Zhongshan Road, Dalian 116023, China
e-mail: wangjh@dicp.ac.cn
e-mail: taozhang@dicp.ac.cn

K. Zhao · F. Yu
Graduate University of Chinese Academy of Sciences, Beijing 100049, China

X. Liu · C. Jin · A. Rykov · J. Wang · T. Zhang
Mössbauer Effect Data Center, Dalian Institute of Chemical Physics,
Chinese Academy of Sciences, 457 Zhongshan Road, Dalian 116023, China

recycle in reaction medium by adding an external magnetic field [1–4]. However the magnetic iron oxide particles tend to be eroding, especially in acid environment, and to be aggregating during reaction. To avoid these undesired disadvantages, different protection shells were developed: surrounding by the terminal phosphoric acid [1]; coating with inert materials such as silica [2] or hydroxyapatite (HAP) [3]; modifying by ionic liquid [4]. Unfortunately, for these catalysts mentioned above, the active sites and the support are isolated, and the iron oxide only plays a role in magnetic separation. Actually, the support has an excellent capability in promoting the catalytic activity of the active component [5]. Especially, when the active component was support sensitive, like gold, different crystal structures of the same oxide show quite different catalytic performances [6].

In our previous work, we designed a highly active gold catalyst, Au/FeO_x-HAP, with strong sintering-resistance and excellent durability under reaction atmosphere [7]. Further characterizations revealed that gold deposited on the juncture of FeO_x and HAP, and the FeO_x in Au/FeO_x-HAP were mainly existed as maghemite even after calcination at 600 °C (to be published soon in detail).

In this study, with the assistance of ⁵⁷Fe Mössbauer and X-ray absorption near edge structure (XANES) spectroscopic techniques, we make further investigation on the influence of HAP on maghemite-to-hematite phase transfer.

2 Experimental

2.1 Composites preparation

The detail of preparation of FeO_x and FeO_x-HAP were reported elsewhere [7]. For FeO_x, denoted by F, the samples as synthesized and further calcined at 300, 400, 500 °C for 6 h were denoted as F-FD, F-300, F-400 and F-500 respectively in this work. FeO_x-HAP (FH) with different contents of FeO_x (12, 25, 50 and 75 wt.%) were prepared by using the proper amount of precursor (initial iron solution (0.185 M)/ammonia water = 2 V/1 V, Ca²⁺ solution/PO₄³⁻ solution = 1 V/1 V, total volume was about 200 mL). The samples as synthesized and further calcined at 400, 500, 600 °C for 6 h were denoted as xxFH-FD, xxFH-400, xxFH-500 and xxFH-600 respectively in this work (xx represents FeO_x content).

2.2 Characterizations

The transmission electron microscopy (TEM) image was observed on a JEOL JEM-2000EX microscope operated at 120 kV. The ⁵⁷Fe Mössbauer spectra of the prepared samples were recorded at 80 K or room temperature on a Topologic 500A spectrometer, the ⁵⁷Co(Rh) source is moving in a constant acceleration model. To get the best fitted results, some samples were fitted by the γ -Fe₂O₃ model with QS = 0, and full line width at half maximum ($W_{1,6} = W_{2,5} + C = W_{3,4} + 2C$, C equals to constant). The XANES spectra were made at the BL14W1 beamline of SSRF, SINAP (Shanghai, China) using a fixed-exit double-crystal Si (311) monochromator. The storage ring was operated at 3.5 GeV with injection currents of 100 mA.

Fig. 1 TEM image and magnetic property of 50FH-600 (a); and images of magnetic property for other samples (b)

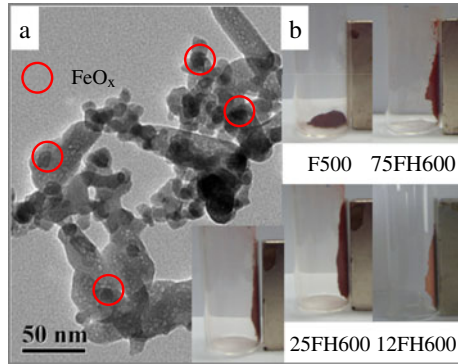
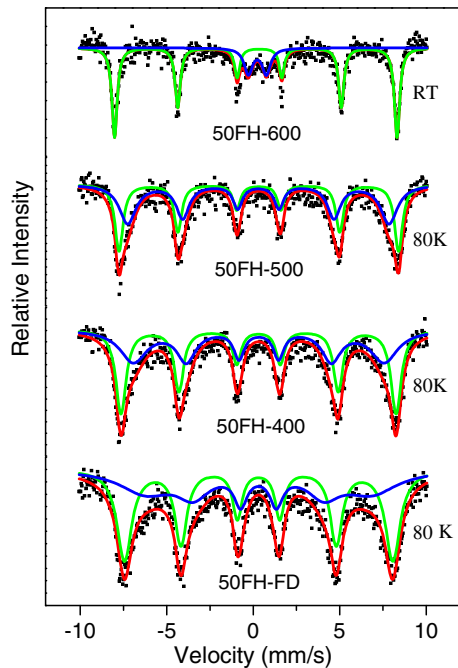


Fig. 2 ^{57}Fe Mössbauer spectra for 50FH sample after different heat treatment



3 Results and discussion

The TEM image of 50FH-600 and magnetic properties of FeO_x -HAP and FeO_x after calcination are shown in Fig. 1. It can be seen that, in an external magnetic field, the FeO_x -HAP composites exhibit a strongly magnetic property even after 600 °C calcination while FeO_x become nonmagnetic after 500 °C heat treatment. The TEM image of 50FH-600 indicates that both FeO_x and HAP are evenly dispersed, and the FeO_x sphere nanoparticles are almost encapsulated in HAP due to the strong interaction between FeO_x surface and phosphate radical of HAP [8].

The ^{57}Fe Mössbauer and Fe K-edge XANES were performed on 50FH and FeO_x samples to get an understanding of the influence of HAP on maghemite-to-hematite

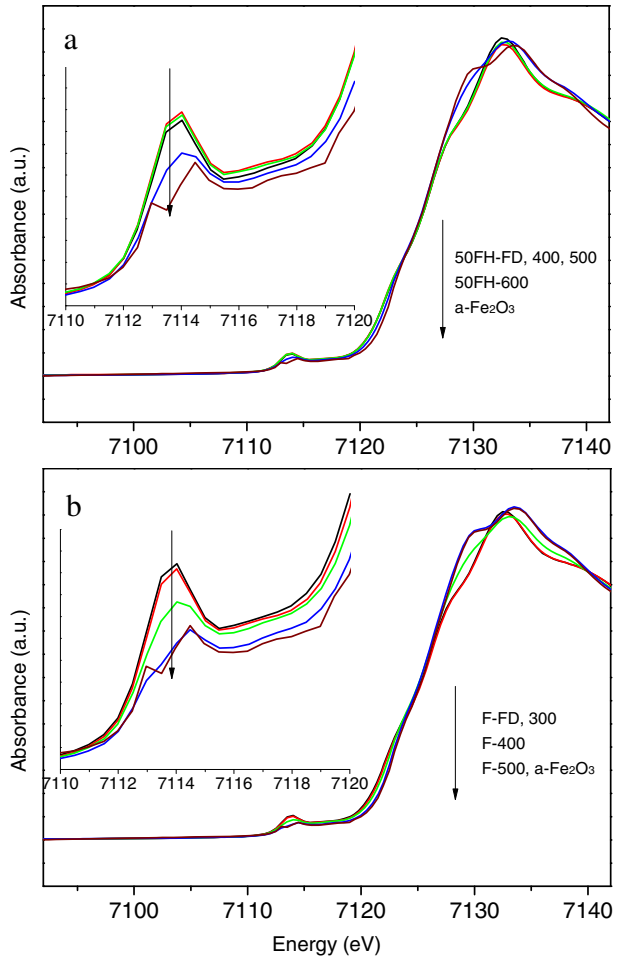
Table 1 ^{57}Fe Mössbauer parameters of 50FH and F at 80 K

Sample	Oxidation state of iron	IS ^a mm s ⁻¹	QS ^b mm s ⁻¹	B _{hf} T	Spectral area % ^c	Component
50FH-FD	Fe ³⁺	0.31		48.2	53.3	$\gamma\text{-Fe}_2\text{O}_3$
	Fe ³⁺	0.31		40.6	46.7	
50FH-400	Fe ³⁺	0.31		49.4	50.1	$\gamma\text{-Fe}_2\text{O}_3$
	Fe ³⁺	0.32		45.1	49.9	
50FH-500	Fe ³⁺	0.32		50.2	45.3	$\gamma\text{-Fe}_2\text{O}_3$
	Fe ³⁺	0.30		47.0	54.7	
50FH-600 ^d	Fe ³⁺	0.26	-0.21	50.6	81.3	$\alpha\text{-Fe}_2\text{O}_3$
	Fe ³⁺	0.24	1.04		18.7	
F-FD	Fe ³⁺	0.31		48.7	41.2	$\gamma\text{-Fe}_2\text{O}_3$
	Fe ³⁺	0.31		44.2	58.8	
F-300	Fe ³⁺	0.33		50.1	35.3	$\gamma\text{-Fe}_2\text{O}_3$
	Fe ³⁺	0.30		47.3	64.7	
F-400 ^d	Fe ³⁺	0.25	-0.23	51.1	100	$\alpha\text{-Fe}_2\text{O}_3$
F-500 ^d	Fe ³⁺	0.25	-0.22	51.4	100	$\alpha\text{-Fe}_2\text{O}_3$

^aIS Isomer shift; ^bQS Electric quadrupole splitting; ^cUncertainty is $\pm 5\%$ of reported value; ^dRoom temperature

phase transfer in considering that both of them are sensitive to local geometries and electronic structure of atoms in the composite. Figure 2 shows the ^{57}Fe Mössbauer spectra of 50FH calcined at different temperatures and the corresponding parameters are summarized in Table 1. The results indicate that all the 50FH samples calcined below 500 °C are pure $\gamma\text{-Fe}_2\text{O}_3$. Both of the magnetic hyperfine fields enlarged with the increase of calcination temperature indicating that the crystalline phase of $\gamma\text{-Fe}_2\text{O}_3$ becoming perfect while temperature increasing. When the sample is heated up to 600 °C, the poorly crystalline and surface species disappeared and $\gamma\text{-Fe}_2\text{O}_3$ transformed to $\alpha\text{-Fe}_2\text{O}_3$. Differences are also observed in Fe K-edge XANES (Fig. 3a). The pre-edge peak is due to the quadrupole transition of 1s to 3d orbitals, contributed by distorted octahedral coordination Fe sites (*Oct*) and tetrahedral coordination Fe sites (*Tet*), but for $\alpha\text{-Fe}_2\text{O}_3$ there is only distorted *Oct* [9]. Much higher pre-edge peaks for 50FH-FD, 50FH-400 and 50FH-500 than that of $\alpha\text{-Fe}_2\text{O}_3$ indicating further the co-existence of *Tet* and distorted *Oct* sites, the pre-edge peak for 50FH-600 is also higher than that of $\alpha\text{-Fe}_2\text{O}_3$ due to having more or progressively distorted *Oct* which resulted in higher magnetization. Since the iron oxides are almost encapsulated in HAP and the surface modifiers can recover the under-coordinated Fe surface sites back to a bulk-like lattice structure with octahedral sites, the distorted *Oct* should be the interior lattice configuration [10]. Figure 4 and Table 1 depicted the ^{57}Fe Mössbauer spectra and corresponding parameters of FeO_x , the results indicate that F-FD and F-300 are pure $\gamma\text{-Fe}_2\text{O}_3$. With increasing the calcination temperature, the crystalline phase of $\gamma\text{-Fe}_2\text{O}_3$ became perfect which resulted in the enlarged magnetic hyperfine fields. When the calcination temperature was higher than 400 °C, $\gamma\text{-Fe}_2\text{O}_3$ transformed to $\alpha\text{-Fe}_2\text{O}_3$. The Fe K-edge XANES are shown in Fig. 3b, for F-FD and F-300 with the highest pre-edge peak due to co-existence of *Tet* and distorted *Oct* Fe sites. F-400 has a higher pre-edge peak than $\alpha\text{-Fe}_2\text{O}_3$ indicating

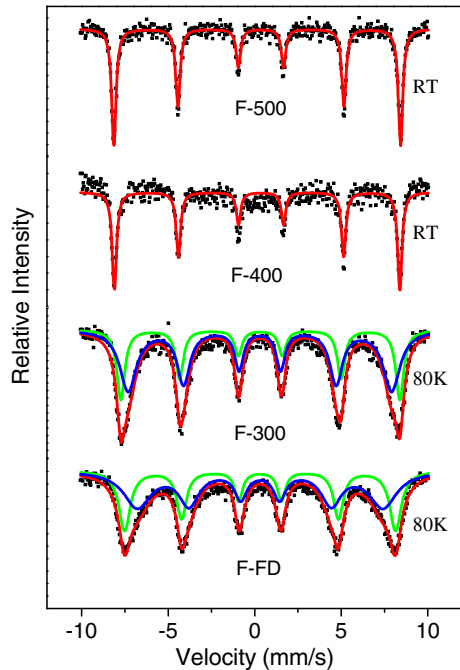
Fig. 3 Fe K-edge XANES spectra for 50FH (a) and F (b) samples after different heat treatment



there are a lot of distorted *Oct* and surface under-coordinate Fe sites. F-500, with almost same intensity of pre-edge peak as α - Fe_2O_3 , indicates that the distorted *Oct* and surface under-coordinated Fe sites decreased with increasing calcination temperature which may be due to the increased size of iron oxide nanoparticles. However, α - Fe_2O_3 exhibits two separated peaks due to electron transition from $1s$ to t_{2g} and e_g sub-bands while for F-500 only a broad peak can be observed. The main reason is that the disorder in the nanoparticle lattice leads to diverse energy levels of the $3d$ orbits [10].

It is a little different compared with our previous results in which there is still much γ - Fe_2O_3 in the Au/FH calcined at 600°C [7]. The presence of gold favors the production of Fe_3O_4 which will be further oxidized to γ - Fe_2O_3 when suffering heat treatment [11].

Fig. 4 ^{57}Fe Mössbauer spectra for F samples after different heat treatment



4 Conclusions

In conclusion, there is strong interaction between HAP and nano iron oxide particles surfaces and the interaction imposed by HAP can stabilize the size and crystal phase of $\gamma\text{-Fe}_2\text{O}_3$. During heat treatment, the interaction imposed by HAP could produce large amounts of distorted octahedral coordination Fe sites in the interior lattice and result in strong magnetic properties. The thermally stable $\gamma\text{-Fe}_2\text{O}_3$ -HAP may provide a new opportunity for developing efficient supported crystal-dependent catalysts.

Acknowledgements Financial support obtained from the Chinese Academy of Sciences for “100 Talents” Project, the National Natural Science Foundation of China (No. 11079036) and the Natural Science Foundation of Liaoning Province (No. 20092173) is greatly acknowledged. The authors would like give special thanks to the staff of 14 W line station of SSRF for giving assistance to the XAFS data collection.

References

1. Zhu, Y., Ship, C.P., Emi, A., Su, Z., Monalisa, Kemp, R.A.: *Adv. Synth. Catal.* **349**(11–12), 1917–1922 (2007)
2. Zhou, L., Gao, C., Xu, W.: *Langmuir* **26**(13), 11217–11225 (2010)
3. Mori, K., Kanai, S., Hara, T., Mizugaki, T., Ebitani, K., Jitsukawa, K., Kaneda, K.: *Chem. Mater.* **19**(6), 1249–1256 (2007)
4. Abu-Reziq, R., Wang, D., Post, M., Alper, H.: *Adv. Synth. Catal.* **349**(13), 2145–2150 (2007)
5. Tsubota, S., Nakamura, T., Tanaka, K., Haruta, M.: *Catal. Lett.* **56**(2–3), 131–135 (1998)

6. Mizera, J., Spiridis, N., Socha, R., Grabowski, R., Samson, K., Korecki, J., Grzybowska, B., Gurgul, J., Kepinski, L., Malecka, M.A.: *Catal. Today* **187**(1), 20–29 (2012)
7. Zhao, K., Qiao, B., Wang, J., Zhang, Y., Zhang, T.: *Chem. Commun.* **47**(6), 1779–1781 (2011)
8. White, M.A., Johnson, J.A., Koberstein, J.T., Turro, N.J.: *J. Am. Chem. Soc.* **128**(35), 11356–11357 (2006)
9. Mori, K., Kondo, Y., Morimoto, S., Yamashita, H.: *J. Phys. Chem. C* **112**(2), 397–404 (2008)
10. Chen, L.X., Liu, T., Thurnauer, M.C., Csencsits, R., Rajh, T.: *J. Phys. Chem. B* **106**(34), 8539–8546 (2002)
11. Jimenez-Lam, S.A., Cardenas-Galindo, M.G., Handy, B.E., Gomez, S.A., Fuentes, G.A., Fierro-Gonzalez, J.C.: *J. Phys. Chem. C* **115**(47), 23519–23526 (2011)